Independent cross sections of Na, K, Rb, Cs, and Fr isotopes produced in Ta and U targets bombarded by ^{12}C ions up to 77 MeV/nucleon

M. de Saint Simon, S. Haan, G. Audi, A. Coc, M. Epherre, P. Guimbal, A. C. Mueller, C. Thibault, and F. Touchard
Laboratoire René Bernas du Centre de Spectrométrie Nucléaire et de Spectrométrie de Masse, 91406 Orsay, France

M. Langevin
Institut de Physique Nucléaire, 91406 Orsay, France

(Received 12 July 1982)

Isotopic distribution measurements for Na, K, Rb, Cs, and Fr in the reactions $^{181}Ta(^{12}C,X)Na,K,Rb,Cs$ and $^{238}U(^{12}C,X)Na,K,Rb,Cs,Fr$ at different energies $E=13$, 27, and 77 MeV/nucleon are reported. The independently observed yields of Rb and Cs show an important contribution for neutron-deficient nuclei. The U target shows very broad isotopic distributions which may be understood as a sum of two components. The results are compared to those obtained by nuclear reactions induced by protons over a wide energy range.

[NUCLEAR REACTIONS $^{181}Ta(^{12}C,X)Na,K,Rb,Cs$; $^{238}U(^{12}C,X)Na,K,Rb,Cs,Fr$; $E=13$, 27, 77 MeV/nucleon; measured Na, K, Rb, Cs, Fr isotopic distributions, heavy ion induced fission, spallation, on-line mass spectrometry.]

I. INTRODUCTION

For more than 10 years, on-line mass spectrometers have been used successfully for the investigation of the isotopic distributions of residues in nuclear reactions induced by neutrons, protons, or heavy ions. This experimental technique provides an accurate determination of the relative cross sections for alkali elements even for short-lived species and is thus complementary to the extensive measurements on the long-lived products undertaken by radiochemistry.[1]

The new possibility to accelerate ^{12}C at 86 MeV/nucleon at the CERN synchrocyclotron was tempting to measure the isotopic distribution data for this projectile energy. Such an intermediate heavy ion energy should correspond to a transition between the low energy range, dominated by complete fusion and transfer reactions, and the relativistic energy range where direct nucleon-nucleon interaction is the principal reaction channel.[2]

The aim of this study concerns two topics: first, to get information about reaction mechanisms in the new energy range, thus studying the behavior of nuclear matter at energies close to physical thresholds such as the sound velocity or the boiling temperature. The second topic concerns the survey of the production of nuclei far from stability leading to further information for nuclear structure physics.

II. EXPERIMENT

A. Experimental procedure

The method is basically the same as described in earlier publications.[3,4] The target-oven assembly (Fig. 1) includes a thin wall (0.5 mm) cylindric graphite oven and a stack of thin graphite foils (5 mg/cm^2). A layer (1 mg/cm^2) of target material is deposited on the surface of every third foil. These "target foils" are separated from each other by two graphite foils used as catchers. The assembly consists of 30 target foils and 60 catchers, where each foil is separated from the neighboring one by a 0.3

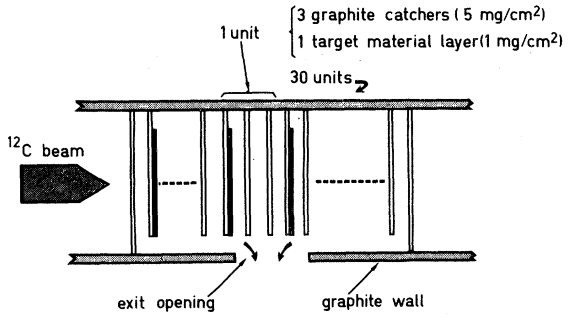

FIG. 1. Schematical view of the target-oven assembly.

mm thick built-in support ring. The large thickness ratios between graphite and target material and between open space and catchers are suitable to get a fast release time combined with a good efficiency. The useful diameter of the foils is 12 mm, several times larger than the ^{12}C beam diameter.

Among the nuclear reaction products being stopped by the catcher foils, the alkali isotopes are escaping preferentially by thermal diffusion through a widely opened exit channel which provides a fast transfer to the ionizing section. This ionizer consists of an elbow duct with a square entrance in front of the exit of the graphite oven. Choosing an appropriate material for the ionizer (re for Na and Ta for the heavier alkalies) and heating it to about 1700 °C, a good chemical selectivity for the alkali isotopes is obtained by the mechanism of surface ionization. Typical efficiencies are evaluated to 30%, 15%, 35%, 75%, and 75% for Na, K, Rb, Cs, and Fr, respectively. The background due to contamination of natural abundant isotopes can be strongly reduced by heating out both target and ionizer at 1800 °C for several days. The exit slit of the elbow duct (1 mm wide) is adapted to the following optics which accelerates the ion beam to 10 keV. The mass separation is achieved in homogeneous magnetic field, deflecting the beam by 90° (radius = 35 cm). High-sensitivity measurements require a location of the detection in a low-background area. Therefore after a 60° electrostatic deflection, the beam passes through a 3.5 m thick concrete shielding (Fig. 2), thus hindering direct view of the target area from the detectors. Beam guidance is provided by two quadrupole triplets.

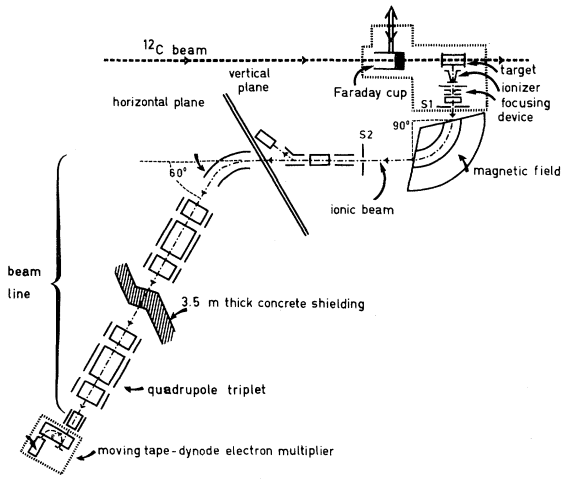

FIG. 2. View of the setup on-line to the synchrocyclotron.

Finally, the beam is detected at the end of the beam line by ion counting with an electron multiplier whose first dynode is a moving tape system.[5] In this way, parasitic counts due to the decay of radioactive isotopes or their daughters are avoided. The whole system has a transmission of better than 80%.

The apparatus is set up on-line to the CERN synchrocyclotron. The energy of the external C^{4+} beam, being initially 86 MeV/nucleon, is reduced to 82.5 MeV/nucleon at the entrance of our target owing to different vacuum tight windows located in the ^{12}C beam line. The projectile energy can be changed by carbon degraders set directly at the exit of the accelerator, taking advantage of its focusing line to get a noncontaminated beam on the target. The beam intensity is measured periodically by a removable Faraday cup located just in front of our target. The cyclotron beam can be pulsed in order to allow for cyclic measurements of the residual background.

The timing of the measurements is chosen according to the characteristics of the diffusion process ($\tau_{1/2} \simeq 50$ ms), and in order to eliminate the contribution from slow diffusion, as well as alkali production by decay of cumulative products in the target assembly or background. The time interval between measurements with beam on and beam off is 2 s and each of them lasts 1 s. The full cycle (4s) is repeated as many times as necessary to get sufficient statistics for the mass spectra. These spectra are obtained by modulating the acceleration voltage of the ion source and of the beam line with a 40 Hz triangular-shaped sweep at a constant magnetic field. The sweep amplitude is adjusted to scan three to five masses. The full mass range of an isotopic distribution is covered by successively changing the magnetic field in order to provide calibration by at least two overlapping masses. To check consistency each complete measurement is repeated at least twice.

B. Data treatment

In order to get the relative yields the spectra "beam off" are subtracted from the "beam on" measurements so that one gets rid of untrue events. The relative heights H of the different peaks lead to the relative yields. The different mass spectra are normalized by using the mass overlaps. In addition the coherence with the measured heavy ion beam intensity is checked. Three corrections have then to be done:

(i) An isotopic discrimination mainly due to high voltage sweeping is determined by comparison with known isotopic ratios. It has been related to the mass difference ΔA according to the formula:

$$\frac{\Delta H}{H}=3\times\frac{\Delta A}{A},$$

where H is the height of the peak.

(ii) The second correction takes into account the β decay of isotopes of interest during the diffusion process. This correction is noticeable for half-lives shorter than 2 s. For $T_{1/2}=200$ ms it can reach 30%.

(iii) The last correction concerns the cumulative effect due to β decay of several generations of parents inside the target. Most of this effect is removed by the difference between beam on and beam off mass spectra. For the half-lives shorter than 10 s, however, we estimate the parent's cross section using the unchanged charge density (UCD) assumption and calculate the subsequent correction with a computer code. This correction is generally negligible and always smaller than 4%.

In most cases the accuracy is limited by statistics, particulary on the wings of the isotopic distributions. The error estimation contains the statistical error with its propagation along the isotopic distribution.

In order to deduce absolute cross sections from the relative independent yields, the efficiency of the device has to be known accurately. This was achieved through radiochemically measured cross sections of doubly shielded isotopes: ^{86}Rb and ^{132}Cs, or after correction for the cumulative effect, ^{24}Na and ^{42}K. These measurements were done by Lund *et al.*[6] with an experimental error estimated at 10%. This uncertainty is included in the cross section results.

III. RESULTS

A. Targets

Two targets have been studied. The uranium target was made of pure ^{238}U prepared by electromagnetic isotope separation. The natural tantalum target can be considered as monoisotopic (^{180}Ta$\simeq 10^{-3}\times{}^{181}$Ta). It was prepared by direct evaporation of bulk metal onto the graphite foils. The total thickness of U and Ta is 30 mg/cm.^{2} That of graphite is 450 mg/cm^2, thus producing an important energy spread of the projectile.

B. ^{12}C beam

The beam energy of the cyclotron can be changed by additional installation of 5 and 8 mm thick graphite degraders. Using the range table of Hubert *et al.*,[7] the mean energy has been estimated at the entrance and at the exit of the two target assemblies (Table I). When the energy at the exit is lower than the Coulomb barrier, this latter value is indicated instead, and the "useful thickness" of the target is calculated (5th column of Table I). In the following each beam energy is referred to by its mean value as indicated in Table I. The beam intensity was 3×10^{11} particle/s at full energy, about 25% lower at the medium energy and 40% lower at the lowest one.

TABLE I. Projectile energies in the laboratory system at the entrance of the target (E_{max}) and at the exit of the target (E_{min}) when E_{min} is larger than the Coulomb barrier. Otherwise the value of the Coulomb barrier (*) is given. E_{mean} is the mean value of the projectile energy (above the Coulomb barrier) in the target assembly. The useful thickness of the target corresponds to the part of the target where the projectile energy is larger than the Coulomb barrier.

Target	E_{max} (MeV/nucleon)	E_{min} (MeV/nucleon)	E_{mean} (MeV/nucleon)	Useful thickness of target (mg/cm^2)
^{238}U	82.5	71.3	77	30
	39.2	13.7	27	30
	25.3	5.8*	13	13
^{181}Ta	82.5	71.3	77	30
	39.2	13.7	27	30
	25.3	5.0*	13	14

TABLE II. Independent cross sections of Na and K in $^{12}C + ^{238}U$ and $^{12}C + ^{181}Ta$ systems. The ^{39}K and ^{41}K are not measurable because the natural background is too important. ^{24}Na has been corrected for the contribution of the carbon target (see text). The absolute cross sections are obtained by radiochemical determination of ^{24}Na and ^{42}K due to the measurements of Lund *et al.* (Ref. 6).

	U target cross section (mb)			Ta target cross section (mb)		
Isotope	77 MeV/nucleon	27 MeV/nucleon	13 MeV/nucleon	77 MeV/nucleon	27 MeV/nucleon	13 MeV/nucleon
Na 24	2.8 ±0.3	0.33±0.09	0.23±0.06	2.5 ±0.2	0.36±0.04	
25	3.2 ±0.3			2.2 ±0.3	0.32±0.14	
26	1.4 ±0.3			0.83 ±0.21		
K 38				0.06 ±0.01		
40	0.8 ±0.18	0.24±0.15		2.3 ±0.3	0.13±0.02	
42	2.7 ±0.3	0.57±0.13		2.8 ±0.3	0.18±0.02	0.08±0.02
43	3.2 ±0.3	0.92±0.09		2.2 ±0.2	0.18±0.02	0.09±0.01
44	2.4 ±0.3	0.76±0.16		1.1 ±0.1	0.10±0.01	0.06±0.01
45	1.6 ±0.2	0.56±0.14		0.47 ±0.06	0.04±0.01	
46	0.7 ±0.1	0.24±0.080		0.14 ±0.02	0.01±0.004	
47	0.36±0.11			0.03 ±0.01		
48	0.06±0.07			0.003±0.003		

C. Measurements in the ^{238}U target

The isotopic distributions of Na, K, Rb, Cs, and Fr have been measured. The sodium isotopic distribution is corrected for the contribution due to a reaction with the carbon catcher foils using a blank experiment without target material deposited on the foils. In the carbon target, neutron-deficient sodium isotopes are observed from mass 20 to 24, particularly at the lowest energy. They are produced

Table III. Independent cross sections of Rb isotopes in $^{12}C + ^{238}U$ and $^{12}C + ^{181}Ta$ systems. The absolute cross sections are obtained by radiochemical determination of ^{86}Rb due to the measurements of Lund *et al.* (Ref. 6).

	U target cross section (mb)			Ta target cross section (mb)		
Isotope	77 MeV/nucleon	27 MeV/nucleon	13 MeV/nucleon	77 MeV/nucleon	27 MeV/nucleon	13 MeV/nucleon
Rb 77				0.002±0.001		
78				0.015±0.002	0.001±0.001	
79	0.18±0.07			0.019±0.01	0.015±0.002	
80	0.88±0.19	0.24±0.08		0.49 ±0.005	0.09 ±0.01	0.03±0.005
81	2.9 ±0.5	1.05 ±0.21		1.2 ±0.1	0.34 ±0.04	0.14±0.02
82	6.8 ±1.0	3.1 ±0.5	0.64±0.17	1.9 ±0.2	0.77 ±0.09	0.41±0.05
83	12.9 ±1.8	7.0 ±1.1	1.8 ±0.4	2.3 ±0.2	1.4 ±0.2	0.92±0.11
84	19.5 ±2.7	12.9 ±2.1	3.8 ±0.8	2.2 ±0.2	1.7 ±0.2	1.4 ±0.1
85	28.1 ±3.8	20.5 ±3.2	8.4 ±2.2	1.8 ±0.2	1.7 ±0.2	1.8 ±0.2
86	28.2 ±3.8	19.5 ±2.8	8.8 ±1.6	1.1 ±0.1	1.2 ±0.1	1.4 ±0.2
87	27.4 ±3.5	20.3 ±3.0	10.3 ±2.2	0.52 ±0.07	0.59 ±0.08	0.84±0.11
88	24.1 ±3.1	17.3 ±2.5	10.4 ±1.7	0.20 ±0.03	0.25 ±0.03	0.39±0.05
89	23.2 ±2.7	15.1 ±2.1	10.0 ±1.6	0.06 ±0.01	0.09 ±0.01	0.15±0.02
90	23.6 ±2.7	14.0 ±1.8	9.3 ±1.4	0.02 ±0.01	0.02 ±0.004	0.04±0.007
91	25.7 ±2.6	14.7 ±1.5	9.6 ±1.0	0.007±0.001	0.006±0.001	
92	24.2 ±2.8	12.7 ±1.6	8.6 ±1.2	0.003±0.003	0.002±0.005	
93	19.4 ±2.3	10.6 ±1.5	7.3 ±1.2			
94	11.2 ±1.4	6.1 ±0.9	4.3 ±0.7			
95	5.6 ±0.7	3.2 ±0.5				
96	2.0 ±0.3	1.1 ±0.2				
97	0.60±0.16	0.33±0.14				

TABLE IV. Production cross sections of Cs isotopes in $^{12}C + ^{238}U$ and $^{12}C + ^{181}Ta$ systems. The absolute cross sections are obtained by radiochemical determination of ^{132}Cs due to the measurements of Lund *et al.* (Ref. 6).

	U target cross section (mb)			Ta target cross section (mb)		
Isotope	77 MeV/nucleon	27 MeV/nucleon	13 MeV/nucleon	77 MeV/nucleon	27 MeV/nucleon	13 MeV/nucleon
Cs 118				0.004±0.004		
119				0.043±0.009		
120				0.21 ±0.03		
121	0.14±0.05			0.72 ±0.09	0.005±0.003	
122	0.36±0.07			1.5 ±0.02	0.019±0.006	
123	1.0 ±0.02			2.4 ±0.3	0.55 ±0.011	
124	2.0 ±0.3	0.73±0.25		2.6 ±0.3	0.087±0.015	0.020±0.005
125	4.0 ±0.5	2.2 ±0.5		2.6 ±0.3	0.12 ±0.02	0.034±0.007
126	5.8 ±0.7	4.4 ±0.9	0.92±0.37	1.9 ±0.2	0.14 ±0.02	0.045±0.009
127	7.9 ±1.0	7.6 ±1.4	2.2 ±0.7	1.5 ±0.2	0.12 ±0.01	0.058±0.006
128	9.6 ±1.1	10.5 ±1.8	3.5 ±1.0	0.74 ±0.10	0.085±0.012	0.053±0.011
129	11.0 ±1.1	13.7 ±2.3	5.4 ±1.2	0.43 ±0.07	0.055±0.009	0.037±0.009
130	11.8 ±1.5	16.7 ±1.7	7.2 ±1.5	0.17 ±0.03	0.028±0.007	0.025±0.008
131	11.4 ±1.5	16.4 ±2.6	8.7 ±1.7	0.088±0.019	0.014±0.004	0.013±0.014
132	11.1 ±1.4	14.5 ±2.4	9.0 ±0.9	0.032±0.013	0.003±0.004	0.003±0.004
133	11.3 ±1.8	12.0 ±2.2	10.4 ±1.7			
134	10.6 ±1.8	9.1 ±1.8	7.5 ±1.2			
135	11.1 ±1.9	7.6 ±1.6	6.2 ±1.2			
136	9.6 ±1.6	6.5 ±1.3	4.8 ±1.1			
137	10.9 ±2.1	6.2 ±1.4	5.6 ±1.3			
138	8.9 ±1.7	4.7 ±1.1	3.4 ±0.9			
139	9.5 ±1.9	4.6 ±1.0	4.0 ±1.4			
140	7.6 ±1.6	4.1 ±1.0	2.7 ±1.0			
141	7.6 ±1.6	3.6 ±0.9	2.3 ±0.8			
142	4.4 ±1.0	2.4 ±0.7	1.6 ±0.7			
143	2.8 ±0.7	1.5 ±0.5				
144	0.95±0.24	0.41±0.26				
145	0.32±0.11					
146	0.13±0.09					

near the end of the range of ^{12}C in the natural carbon of the target, in agreement with the observation of Bjørnstad *et al.*[8] At high energy this contribution is strongly decreasing and can be understood as secondary reaction products. The ^{39}K and ^{41}K are not measurable since the natural background is overwhelming. The corresponding cross sections are summarized in Table II. Rb and Cs isotopic distributions are shown in Tables III and IV and plotted in Figs. 3 and 4. The extremely wide isotopic distributions of Rb and Cs covering neutron-deficient as well as neutron-rich isotopes encouraged the choice of a target with a high fission barrier, e.g., the tantalum target (30 MeV).

An isotopic distribution of Fr isotopes could be measured in spite of the small counting rate (Table V). Due to their short half-lives, the isotopes of mass larger than 213 are not detectable. The absolute cross sections are evaluated from the total efficiency of our device. The distribution is centered on the neutron-deficient side, pointing to a spallationlike process which takes place in the nuclei surviving fission.

D. Measurements in the ^{181}Ta target

Na and K isotopic distributions are compiled in Table II. Rb and Cs results are given in Tables III and IV and plotted in Figs. 5 and 6. Immediately, one notices that the behavior of the Rb and Cs isotopic distributions is very different as compared to the U target. Here, the distributions cover essentially the neutron-deficient isotopes, being much narrower than in the former case.

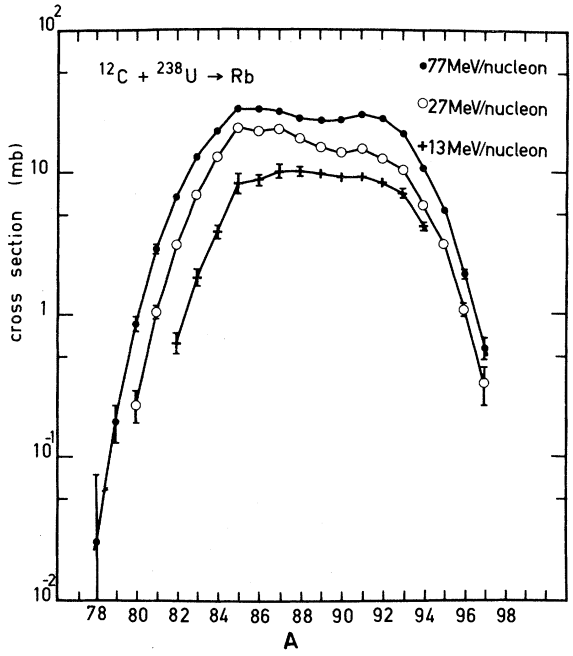

FIG. 3. Isotopic distributions of Rb isotopes produced in the $^{12}C + ^{238}U$ system for three projectile energies.

E. Elementary cross sections

For both studied systems we have calculated the cross sections for the production of K, Rb, Cs, and Fr. The results are compiled in Table VI. The geometrical cross sections for these systems are, respectively, 4.7 and 4.2 b. In the case of U, the production of medium weight nuclei must be dominated by the fission process, in contrast to the tantalum case, where spallation obviously takes place.

TABLE V. Independent cross sections of Fr isotopes in the $^{12}C + ^{138}U$ system.

Isotopes	U target cross section (mb) 77 MeV/nucleon	Isotopes	U target cross section (mb) 77 MeV/nucleon
Fr 206	0.10±0.10	Fr 210	0.90±0.30
207	0.20±0.10	211	1.20±0.50
208	0.45±0.20	212	1.40±0.60
209	0.69±0.20	213	1.50±0.60

IV. DISCUSSION

A. Comparison with proton induced reactions

Figures 7 and 8 show a comparison of Rb and Cs isotopic distributions obtained in U target bombardments by 77 MeV/nucleon ^{12}C and protons of vari-

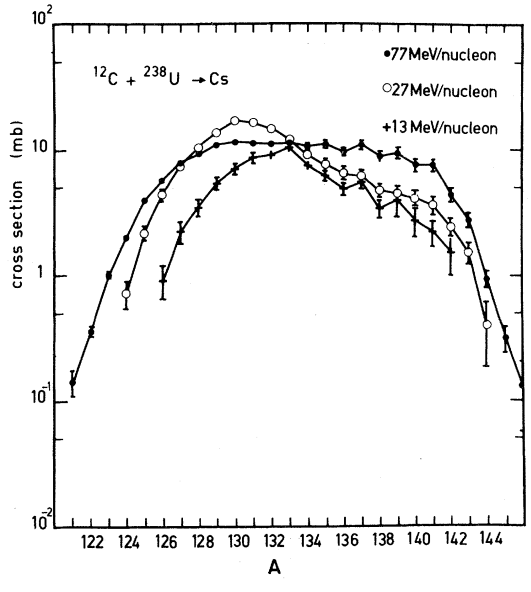

FIG. 4. Isotopic distribution of Cs isotopes produced in the $^{12}C + ^{238}U$ system for three projectile energies.

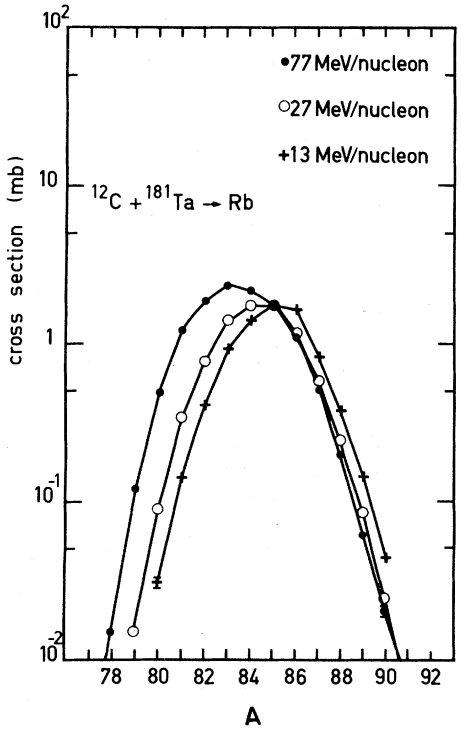

FIG. 5. Isotopic distribution of Rb produced in the $^{12}C + ^{181}Ta$ system for three projectile energies.

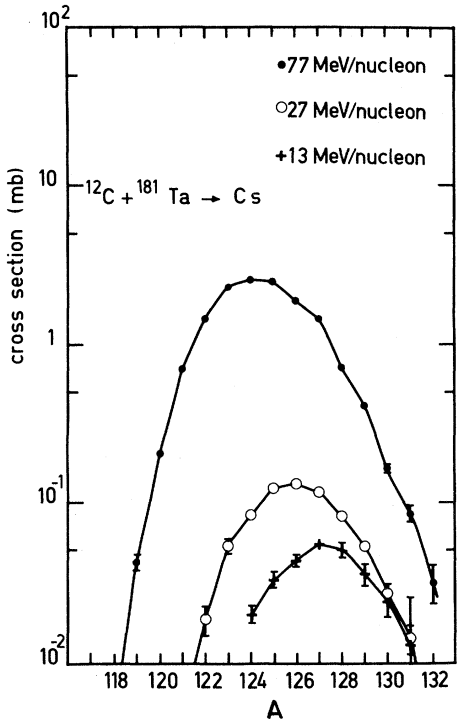

FIG. 6. Isotopic distribution of Cs produced in the $^{12}C + ^{181}Ta$ system for three projectile energies.

ous energies: 40 MeV,[9] 156 MeV,[10] 1 GeV,[11] and 24 GeV.[10] Three features may be pointed out. First, in most cases, the ^{12}C cross sections are the largest; that should be related to the size of the projectile and to the fission enhancement due to a larger angular momentum transfer brought by the heavy ion projectile. From the point of view of the production of exotic nuclei this process is competitive with high-energy proton-induced reactions in spite of the shorter projectile range in the target material for the heavy ions in the case of comparable beam intensities. This condition, which is not fulfilled at the CERN synchrocyclotron SC, should be reached at the GANIL accelerator. The second feature is the resemblance of 77 MeV/nucleon (924 MeV) ^{12}C and 1 GeV protons which underlines the prevalence of the total kinetic energy of the projectile over its energy per nucleon in this energy range. The last feature is the similarity of the neutron-rich wing shapes, suggesting that the same reaction mechanism is involved here.

It would be interesting to do the same type of comparison using the tantalum results. But unfortunately much fewer results with protons are available. In Figs. 9 and 10 we have compared the results for ^{12}C and 24 GeV protons.[10] The narrow isotopic distributions centered on neutron-deficient isotopes are almost similar in shape and in cross section, even though a shift towards the heavy masses is noticeable for the ^{12}C projectile in the Rb distribution. The quite different aspect of the distribution obtained with the two heavy targets is very likely related to their different fission barriers, 6 and 30 MeV,[12,13] respectively.

B. Gaussian fit of the Rb and Cs data

The first conclusions incite us to distinguish between the neutron-rich and the neutron-deficient wings of the Rb and Cs distributions obtained by the U target. From the comparison with the proton induced reaction, we think that the neutron-rich distribution for low energy projectiles, such as 40 MeV protons, is characteristic for any low-energy fission process induced by peripheral collision, whatever is the projectile or its energy.[14] On the contrary, according to a large excitation energy, the neutron-deficient component is attributed to fission and/or evaporation following more central collisions. The shape of the distributions and the statistical aspect of such a phenomenon suggest the attempt of a two Gaussian fit for the U data and a single Gaussian fit for the Ta data.

The deduced parameters such as the center of gravity $\langle A \rangle$, the FWHM, and the total area S of the Gaussian components are summarized for Rb

TABLE VI. Elementary cross section for K, Rb, Cs, and Fr in the $^{12}C + ^{238}U$ and $^{12}C + ^{181}Ta$ systems.

	U target cross section (mb)			Ta target cross section (mb)		
Element	77 MeV/nucleon	27 MeV/nucleon	13 MeV/nucleon	77 MeV/nucleon	27 MeV/nucleon	13 MeV/nucleon
K	11.8± 0.6	3.3±0.3		9.1±0.5	0.70±0.05	0.30±0.03
Rb	287 ±10	180 ±8	93.2±5.0	12.0±0.4	8.2 ±0.4	7.5 ±0.5
Cs	172 ± 7	150 ±7	85.4±8.4	15.0±0.7	0.73±0.04	0.29±0.03
Fr	$\gtrsim 6$					

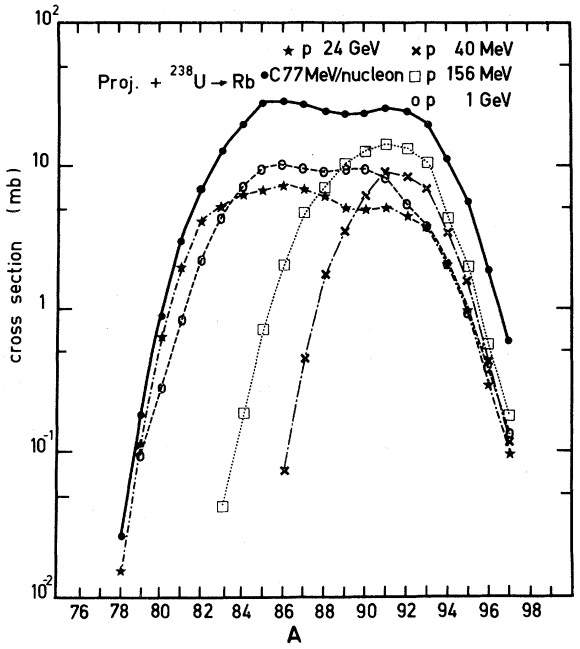

FIG. 7. Isotopic distributions of Rb in the system $^{12}C + ^{238}U$ (this work) compared with the $p + ^{238}U$ system at different energies: 40 MeV (Ref. 9), 156 MeV (Ref. 10), 1 GeV (Ref 11), and 24 GeV (Ref. 10).

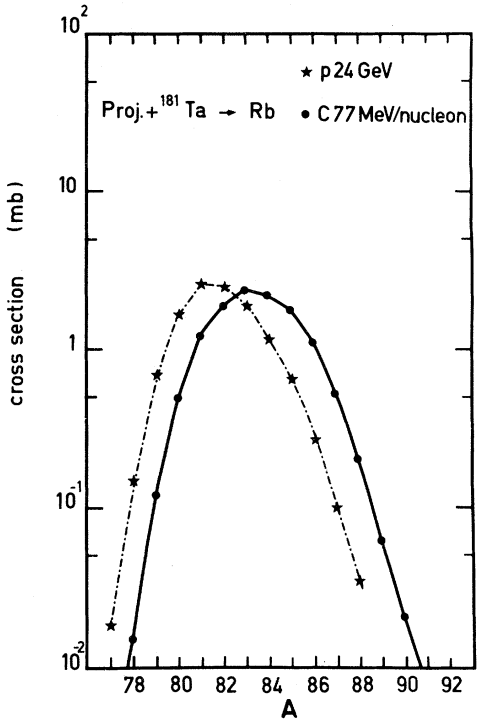

FIG. 9. Isotopic distributions of Rb in the system $^{12}C + ^{181}Ta$ (this work) compared with $p + ^{181}Ta$ system at 24 GeV (Ref. 10).

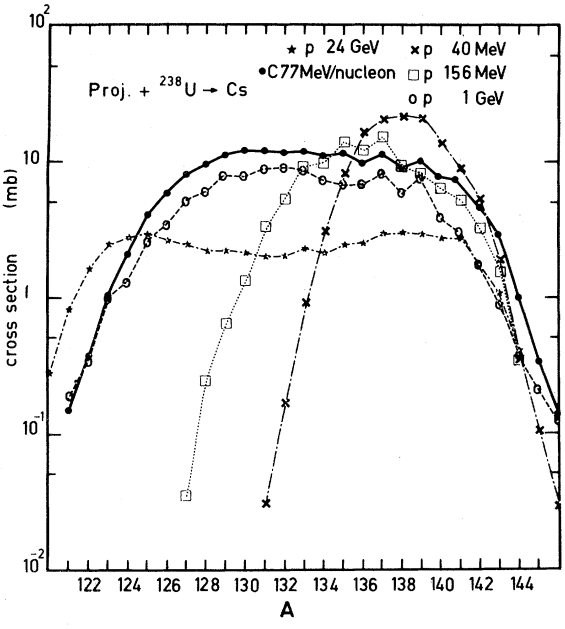

FIG. 8. Isotopic distributions of Cs in the system $^{12}C + ^{238}U$ (this work) compared with the $p + ^{238}U$ system at different energies: 40 MeV (Ref. 9), 156 MeV (Ref. 10), 1 GeV (Ref 11), and 24 GeV (Ref. 10).

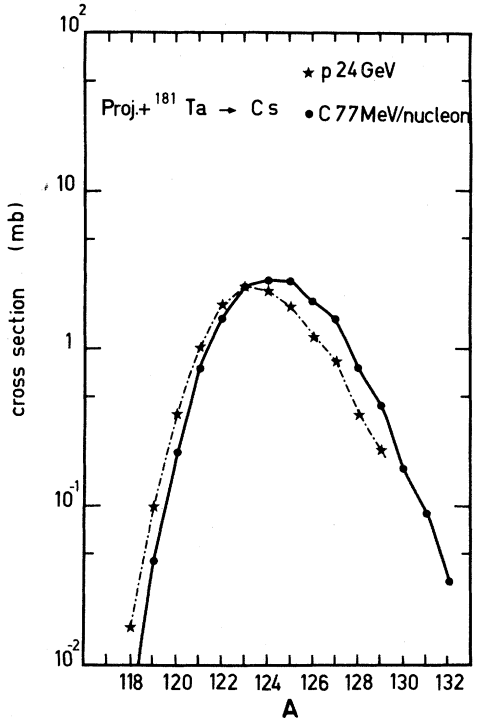

FIG. 10. Isotopic distributions of Cs in the system $^{12}C + ^{181}Ta$ (this work) compared with $p + ^{181}Ta$ system at 24 GeV (Ref. 10).

TABLE VII. Two Gaussian fit of the U + C data. Center of gravity $\langle A \rangle$, width (FWMH), and area (S) of the two components are shown.

Projectile energy MeV/nucleon	Element	Light component $\langle A \rangle$ (u)	FWHM (u)	S (mb)	Heavy component $\langle A \rangle$ (u)	FWHM (u)	S (mb)
77	Rb	85.79±0.03	5.19	165	91.33 ±0.02	4.81	133
	Cs	130.45±0.09	8.12	105	138.75 ±0.12	6.00	59
27	Rb	86.08±0.04	4.97	103	91.45 ±0.02	4.81	67
	Cs	130.90±0.09	7.44	122	139.01 ±0.03	6.00	28
13	Rb	86.75±0.08	4.75	52	91.55 ±0.08	4.63	47
	Cs	132.31±0.14	7.30	70	139.13 ±0.19	5.96	18
40 p[a]	Rb				91.511±0.003	4.28	41.88
	Cs				138.056±0.011	4.94	127.00

[a]40 MeV p + U data from Tracy *et al.* (Ref. 9).

and Cs in Table VII. The quality of the fit is shown in Figs. 11 and 12. The same parameters for the single Gaussian fit of Ta data are compiled in Table VIII and shown in Figs. 13 and 14.

For the heavy component, $\langle A \rangle$ and FWHM are obviously insensitive to the projectile energy and thus are rather similar to 40 MeV proton data,[9] in agreement with a fission of nuclei following a peripheral collision. One may notice that the width is slightly larger than in 40 MeV proton induced reactions and consequently the mean excitation energy should be larger than 20 MeV.[9] The ratios of Rb and Cs total cross sections are completely different for ^{12}C and protons, suggesting that, in our case, Rb and Cs are not complementary fragments. This is an indication of the occurrence of nucleon transfers and intranuclear cascades before the fission.

On the light-component side, however, one may notice a strong effect of the projectile energy on $\langle A \rangle$ and FWHM. The extremely large value of the

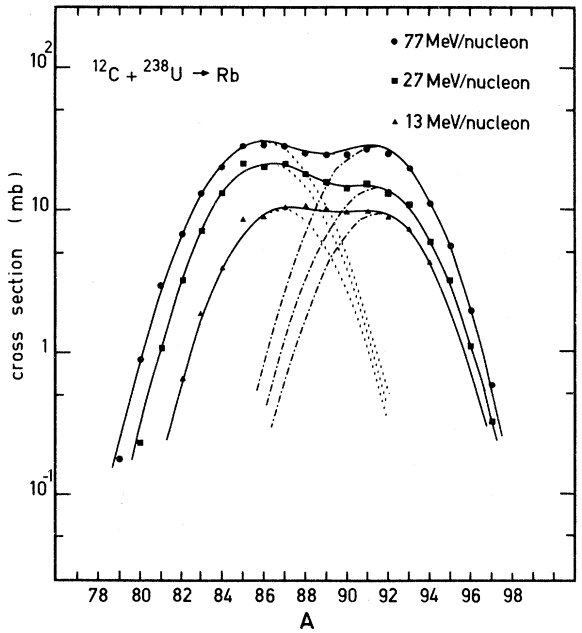

FIG. 11. Two Gaussian fit of Rb data obtained in the ^{12}C + ^{238}U system. The dotted line is the light component, the dashed line shows the heavy component, and the solid line corresponds to the sum of the two Gaussian components.

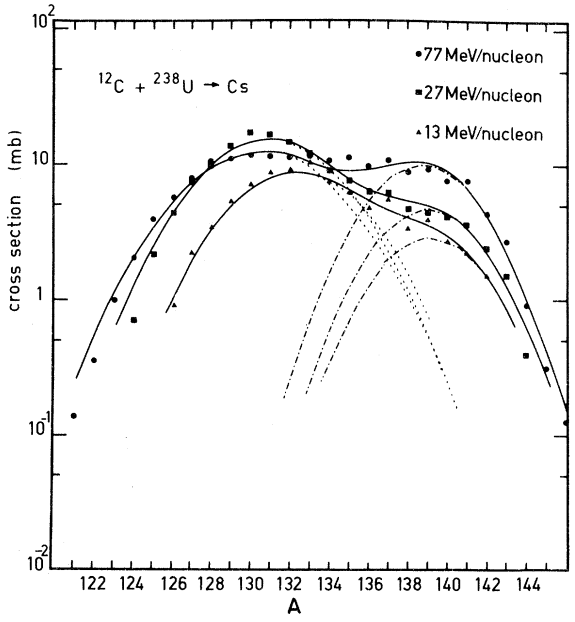

FIG. 12. Two Gaussian fit of Cs data obtained in the ^{12}C + ^{238}U system. The dotted line is the light component, the dashed line shows the heavy component, and the solid line corresponds to the sum of the two Gaussian components.

TABLE VIII. Single Gaussian fit of the Ta + C data.

Projectile energy MeV/nucleon	Element	Single component $\langle A \rangle$ (u)	FWHM (u)	S (mb)
77	Rb	83.61±0.06	4.67	9.48
	Cs	124.58±0.07	5.34	14.05
27	Rb	84.25±0.06	4.20	7.11
	Cs	126.13±0.11	4.97	0.72
13	Rb	84.98±0.06	3.82	7.09
	Cs	127.41±0.23	5.21	0.30

FWHM, particularly in Cs distributions, shows that the two-component fit is no longer realistic. Apparently, more than two Gaussian curves are necessary to reproduce the continuous growth of neutron deficient isotopes. Nevertheless, the low value of the N/Z ratio and the large value of the FWHM show that an important energy transfer from the projectile to the target has taken place. This corresponds to very small impact parameters and may be in competition with a complete explosion of the target nucleus.[15]

The still lower $\langle A \rangle$ values observed for the Ta target are in agreement with the lower N/Z ratio of this element as compared to the case of U. Here the rather small FWHM values are in accordance with the strong limitation to the fission process owing to the high fission barrier. The relatively large total cross section for Cs indicates, however, that there is an important contribution of spallation without fission for the largest ^{12}C energy.

For a more complete analysis of these data, it would be interesting to reproduce the first step of the collision using an intranuclear cascade model,[16] followed by a description of the second step, the deexcitation process, taking into account the competition between evaporation and fission. This last deexcitation channel is crucial when heavy targets are involved in collisions where the angular momentum transfer is important.

V. CONCLUSION

Measurements of independent yields of Na, K, Rb, Cs, and Fr isotopes have been carried out using a mass spectrometer connected on-line to the CERN synchrocyclotron. Bombardments of Ta and U targets with ^{12}C from 13 to 77 MeV/nucleon show broad isotopic distributions of medium mass elements, including neutron-deficient isotopes. The comparison with proton-induced reactions and the striking likeness of 1 GeV protons and 1 GeV ^{12}C

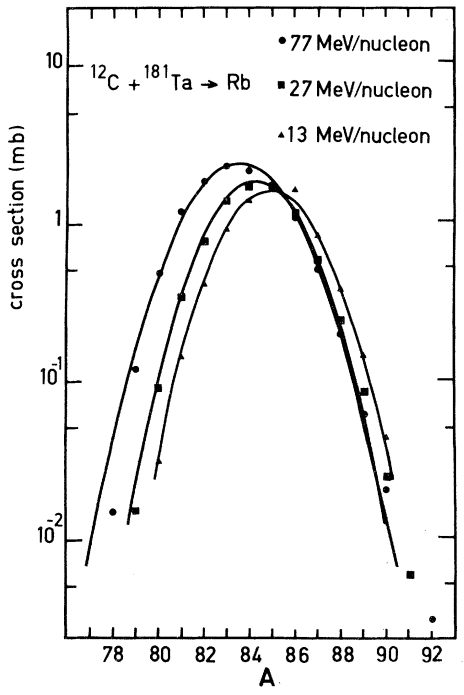

FIG. 13. Single Gaussian fit of Rb data obtained in the $^{12}C + ^{181}Ta$ system (solid line).

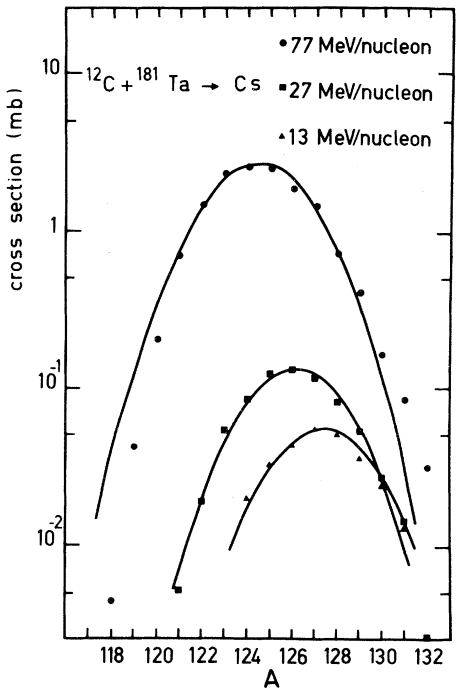

FIG. 14. Single Gaussian fit of Cs data obtained in the $^{12}C + ^{181}Ta$ system (solid line).

demonstrate the prevalence of the total kinetic energy of the projectile over its energy per nucleon.

A two component analysis of the data clearly shows a neutron-rich component independent of the projectile energy, which should be related to peripheral collisions. The strong neutron-deficient component, corresponding to high excitation energy, is related to central collisions followed by fission and spallation. The present work should be completed in terms of comparison with models including fission and spallation processes. From the experimental point of view, other targets and projectiles should be used to test to what extent the parameters which we have determined here are sensitive to the nature of the system.

The cross sections we have observed also seem to be interesting because of production of exotic nuclei. But further investigations are still needed in the fields of projectile fragmentation, reverse systems, and secondary reactions.[17]

ACKNOWLEDGMENTS

The authors are indebted to Dr. E. Hagebø and Dr. T. Lund and co-workers for communicating their cross section measurements prior to publication. We are grateful to the staff of the CERN synchrocyclotron for their efficient operation of the accelerator. It is a pleasure to thank R. Fergeau, M. Jacotin, J. F. Kepinski, and J. Biderman for their contributions in building the experimental equipment and G. Le Scornet for computer programming. One of us, A.C.M., would like to thank the Deutsche Forschungsgemeinschaft and the CNRS for a joint fellowship.

[1]K. Aleklett, D. J. Morrisey, W. Loveland, P. L. McGaughey, and G. T. Seaborg, Phys. Rev. C 23, 1044 (1981).

[2]R. Stock, in *Heavy Ion Collisions,* edited by R. Bock (North-Holland, Amsterdam, 1979).

[3]R. Klapisch, Annu. Rev. Nucl. Sci. 19, 33 (1969).

[4]M. de Saint Simon, L. Lessard, W. Reisdorf, L. Remsberg, C. Thibault, E. Roeckl, R. Klapisch, I. V. Kuznetsov, Yu. Ts. Oganessian, and Yu. E. Penionshkevitch, Phys. Rev. C 14, 2185 (1976).

[5]F. Touchard, G. Huber, R. Fergeau, C. Thibault, and R. Klapisch, Nucl. Instrum. Methods 155, 449 (1978).

[6]T. Lund, E. Hagebø, and I. R. Hardorsen, private communication.

[7]F. Hubert, A. Fleury, R. Bimbot, and D. Gardès, Ann. Phys. (Paris) 5, 1 (1980).

[8]T. Bjørnstad, H. A. Gustafsson, B. Jonson, V. Lindfors, S. Mattsson, A. M. Poskanzer, H. L. Ravn, and D. Schardt, Z. Phys. A 303, 227 (1981).

[9]B. L. Tracy, J. Chaumont, R. Klapisch, J. M. Nitschke, A. M. Poskanzer, E. Roeckl, and C. Thibault, Phys. Rev. C 5, 222 (1972).

[10]J. Chaumont, Ph.D. thesis, Centre National de Recherche Scientifique, Orsay, 1970 (unpublished).

[11]B. N. Belyaev, V. D. Domkin, Yu. G. Korobulin, L. N. Androneko, and G. E. Solyakin, Nucl. Phys. A348, 479 (1980).

[12]H. C. Britt, *Physics and Chemistry of Fission* (IAEA, Vienna, 1979), Vol. 1, p. 3.

[13]R. Vandenbosch and J. R. Huizenga, *Nuclear Fission* (Academic, New York, 1973).

[14]W. Reisdorf, M. de Saint Simon, L. Remsberg, L. Lessard, C. Thibault, E. Roeckl, and R. Klapisch, Phys. Rev. C 14, 2189 (1976).

[15]D. K. Scott, Nucl. Phys. A354, 375 (1981).

[16]H. W. Bertini, T. A. Gabriel, and R. T. Santoro, Phys. Rev. C 9, 522 (1974).

[17]J. P. Dufour, A. Fleury, and R. Bimbot, Phys. Rev. C 23, 801 (1981).